Supporting Information for:

In situ construction of AFe_2O_4/Fe_2O_3 (A=Cd, Ca, Zn) array structures for selective detection of VOCs

Baosheng Li[a,#], Ming Zheng[b,#], Tingting Wang[a], Qiuyue Zheng[a], Ruibai Ma[a], Zoltán Major[c], Xianfa Zhang[a], Lihua Huo[a], Shan Gao[a], Xin Zhou[b,*], Xiaoli Cheng[a,*] and Yingming Xu[a,*]

Key Laboratory of Functional Inorganic Material Chemistry Ministry of Education, College of Chemistry, Chemical Engineering and Materials, Heilongjiang University, Harbin, 150080, China

MIIT Key Laboratory of Critical Materials Technology for New Energy Conversion and Storage, School of Chemistry and Chemical Engineering, Harbin Institute of Technology, Harbin 150000, China

Institute of Polymer Product Engineering, Johannes Kepler University Linz, Austria

E-mail: zhoux@hit.edu.cn, xuyingming@hlju.edu.cn, chengxiaoli@hlju.edu.cn

#: Baosheng Li and Ming Zheng are the first authors of this article.

1. Computation Details.

All calculations were performed based on density functional theory (DFT), as implemented by Vienna Ab initio Simulation Package (VASP)[1, 2]. The interaction between valence electrons and the ionic core described by Projector-augmented wave (PAW)[3, 4], within the exchange-correlation functional was described by Perdew, Burke, and Ernzerhof (PBE)[5]. The D3 correction of Grimme[6, 7] was adopted to compensate for the lack of van der Waals interaction description in the GGA functional. One-electron Kohn−Sham orbitals were expanded with a kinetic energy cutoff of 450 eV. The Brillouin zone was sampled by 2 × 2 × 1, 3 × 3 × 1 and 2 × 3 × 1 Monkhorst-Pack grids of k-points mesh to optimize the surface structure of $ZnFe_2O_4$ (400), $CaFe_2O_4$ (200), and $CdFe_2O_4$ (220) and set the vacuum space to 15 Å in the Z direction to avoid possible image interactions. The convergence criterion for self-consistent iteration was set to 1×10^{-5} eV and the structures were fully relaxed until the final force on each atom was less than 0.03 eV $Å^{-1}$.

[1] J. Hafner, Ab-initio simulations of materials using VASP: Density-functional theory and beyond, 2008. https://doi.org/10.1002/jcc.21057.

[2] G. Kresse, J. Furthmüller, Efficient iterative schemes for ab initio total-energy calculations using a plane-wave basis set, Physical Review B 54(16) (1996) 11169-11186. https://doi.org/10.1103/PhysRevB.54.11169.

[3] G. Kresse, D. Joubert, From ultrasoft pseudopotentials to the projector augmented-wave method, Physical Review B 59(3) (1999) 1758-1775. https://doi.org/10.1103/PhysRevB.59.1758.

[4] P.E. Blochl, PROJECTOR AUGMENTED-WAVE METHOD, Physical Review B 50(24) (1994) 17953-17979. https://doi.org/10.1103/PhysRevB.50.17953.

[5] J.P. Perdew, K. Burke, M. Ernzerhof, Generalized Gradient Approximation Made Simple, Physical Review Letters 77(18) (1996) 3865-3868. https://doi.org/10.1103/PhysRevLett.77.3865.

[6] S. Grimme, S. Ehrlich, L. Goerigk, Effect of the Damping Function in Dispersion Corrected Density Functional Theory, Journal of Computational Chemistry 32(7) (2011) 1456-1465. https://doi.org/10.1002/jcc.21759.

[7] S. Grimme, J. Antony, S. Ehrlich, H.J.J.o.C.P. Krieg, A consistent and accurate ab initio parametrization of density functional dispersion correction (DFT-D) for the 94 elements H-Pu, 132(15) (2010) 154104.

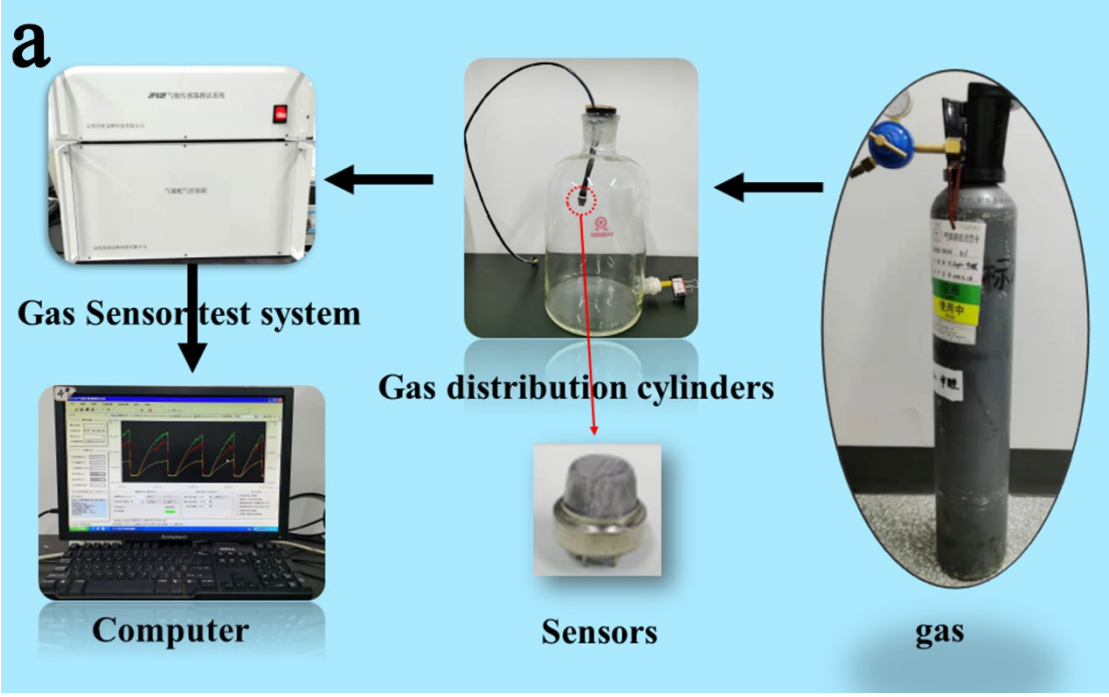

Fig. S1 Schematic diagram of the gas-sensing test device

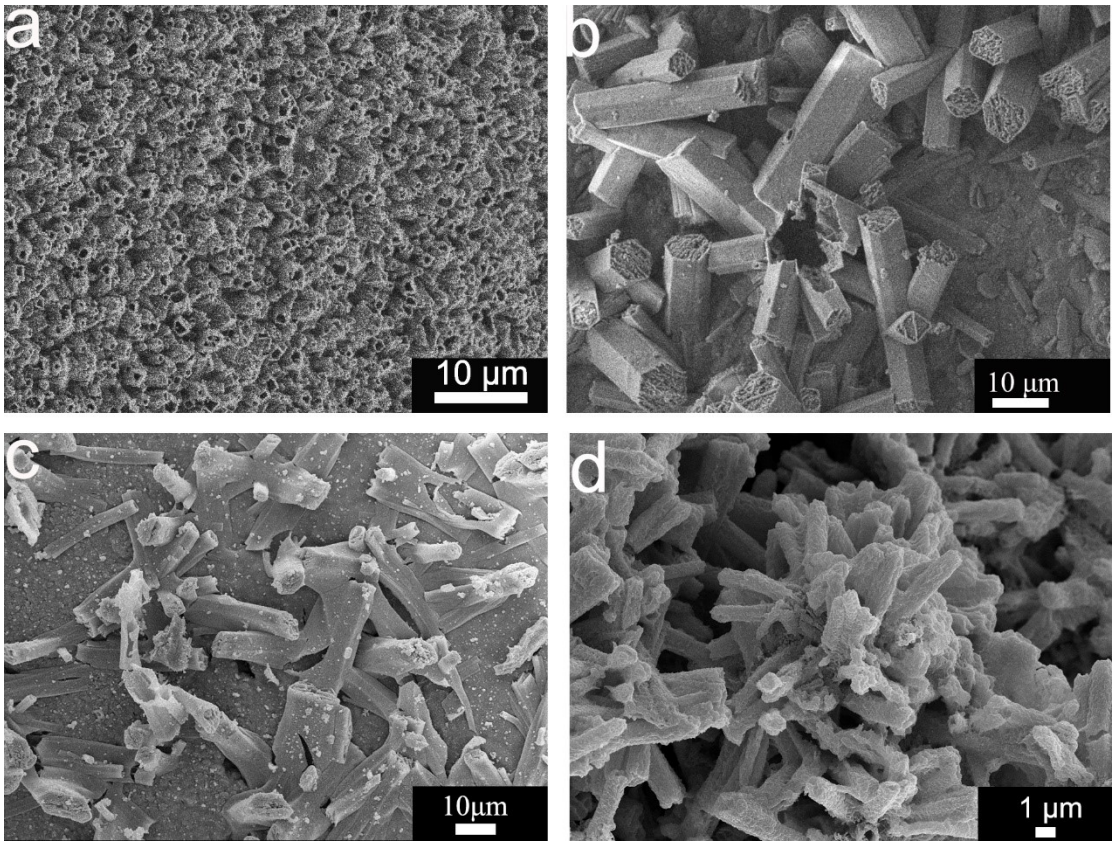

Fig. S2 SEM images of FO-1 (a), FZnFO-3 (b), FCaFO (c) and FCdFO (d) samples

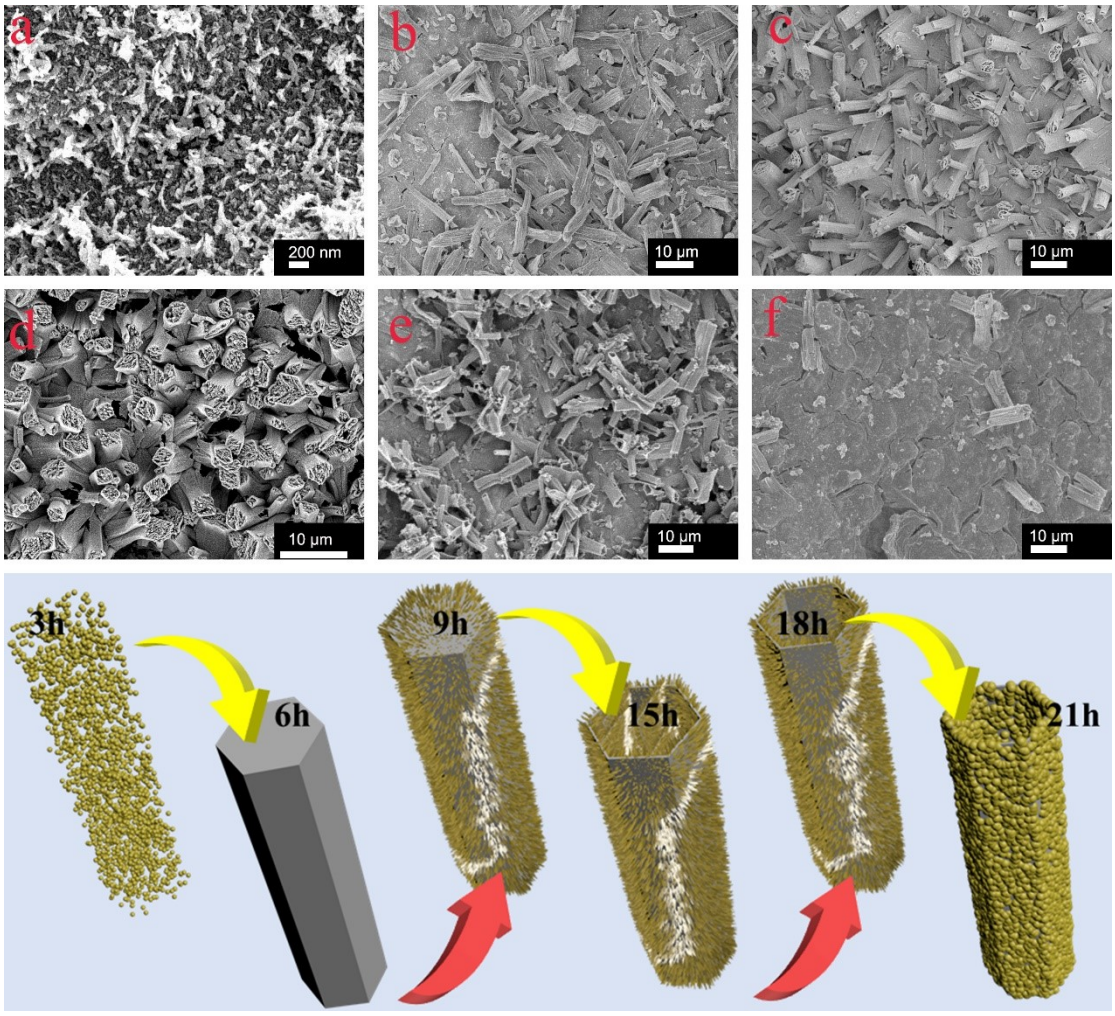

Fig. S3 SEM images of the FZnFO-3 sample obtained at 140 ℃ after different hydrothermal times: 3 h (a), 6 h (b), 9 h (c), 15 h (d), 18 h (e), 21 h (f)

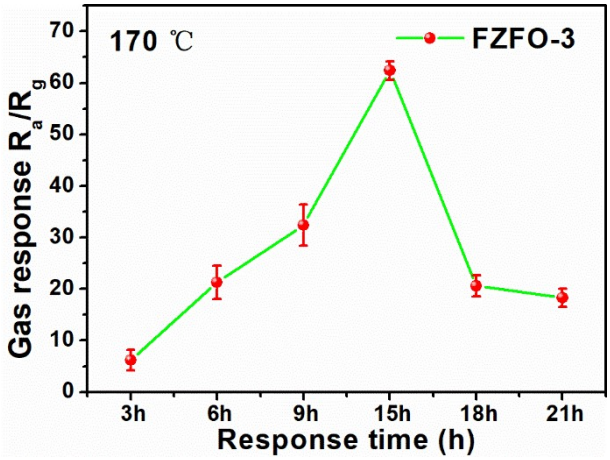

Fig. S4 Response of the FZnFO-3 sample obtained at 140 ℃ after different hydrothermal times for 100 ppm acetone

Fig. S3a shows the SEM of FZnFO-3 sample in the initial stage of the hydrothermal reaction (3h). At this point, it can be clearly seen that the material begins to grow on

the ceramic tube substrate, showing a nanoparticle morphology and no array structure. When the reaction time is increased to 6 h (Fig. S3b), Zn-Fe elements began to grow intertwined, forming a smooth nanorod structure. As the reaction time increases to 9 h, FZnFO-3 gradually forms a nanotube array structure on the substrate (Fig. S3c). When the hydrothermal reaction time is increased to 15 h, the nanotube array is completely formed (Fig. S3d). The nanotube array gradually became sparse and distorted as the reaction time reached 18 h (Fig. S3e). After 21 h of hydrothermal reaction, only a small number of nanotube arrays are present (Figure S3f), indicating that a long hydrothermal reaction time is not conducive to the growth of the array structure. In addition, the FZnFO-3 has the best gas response to acetone at 15 h. Hence, the sensing performance of the composites based on a reaction time of 15 h was further investigated (Fig. S4).

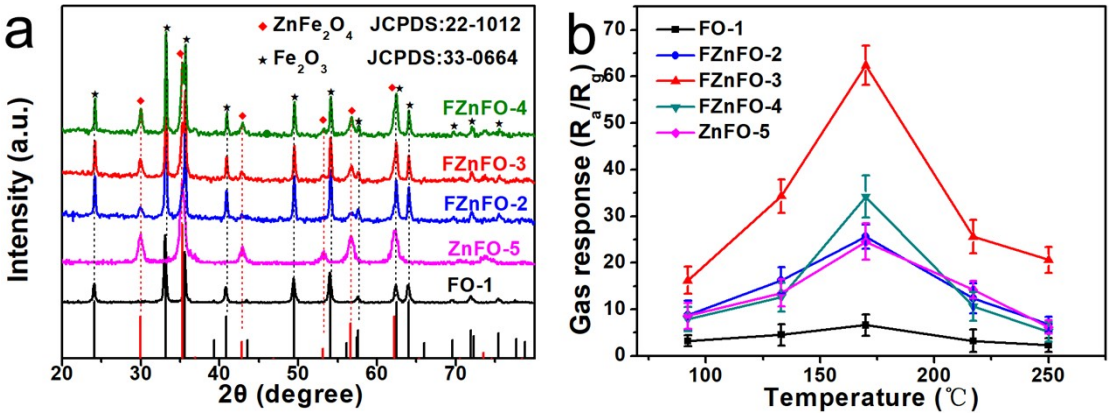

Fig. S5 XRD patterns of Zn: Fe=0:1, 0.1:1, 0.2:1, 0.3:1, 0.5:1 composite (a). Responses (b) of different ratios of composites to 100 ppm acetone

Therefore, five materials were prepared by keeping the 1 mmol $Fe(acac)_3$ content constant and changing the $Zn(acac)_2$ content (0~0.5 mmol) and analyzed by XRD as FO-1, FZnFO-2, FZnFO-3, FZnFO-4, and ZnFO-5 (Fig. S5a). The five sensors showed low responses at 92, and 133 °C, owing mainly to the inability of gas molecules to react effectively with O_{abs} at low temperatures, resulting in low responses (Fig. S5b). As the temperature increases (170 °C), the chemical activity and O_{abs} of the material increase and react rapidly upon contact with the gas, thus improving the gas-sensitive properties. The response decreases with further increases in temperature (217 °C) due to the high

temperature which promotes the desorption of the material from the gas. The testing results indicated that the FZnFO-3 NAs the best sensing performance for acetone (Fig. S5b).

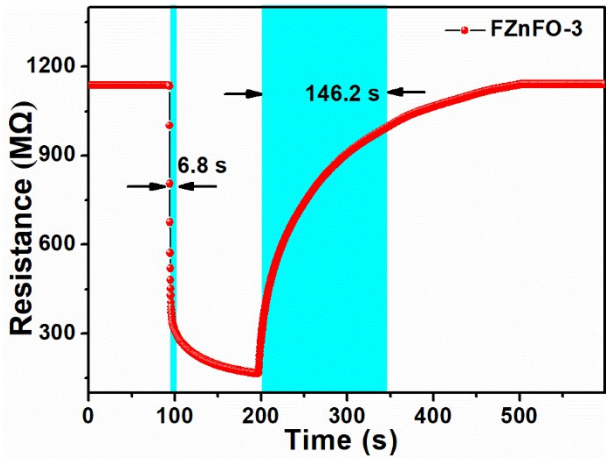

Fig. S6 Single response/recovery curve (c) of FZnFO-3 sensor to 10 ppm acetone at 170 °C

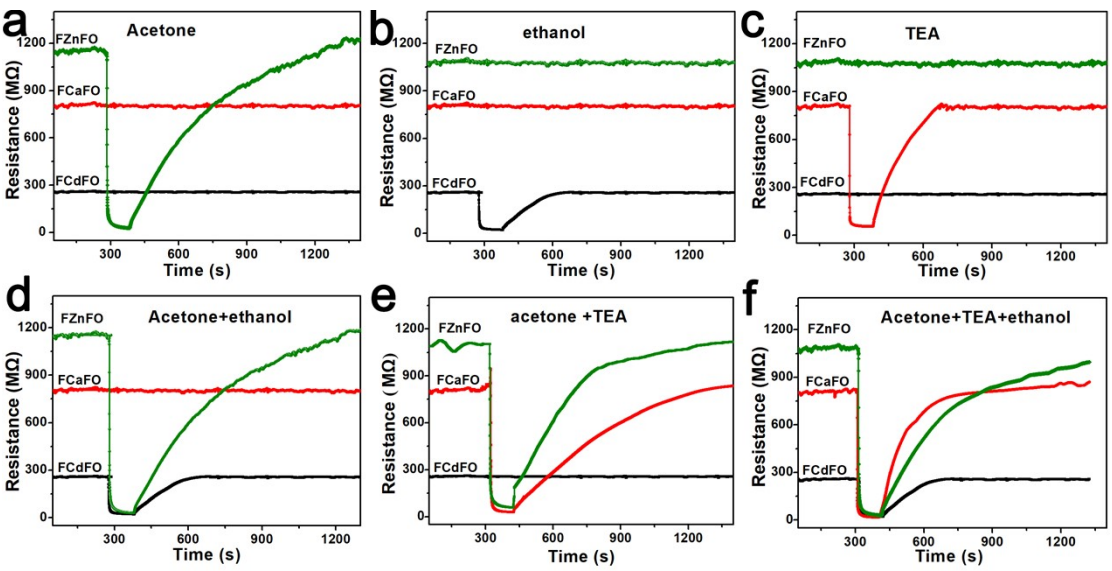

Fig. S7 Cross-test response recovery curves (a-f) of FZnFO, FCdFO, and FCaFO sensors to 100 ppm different mixtures gases

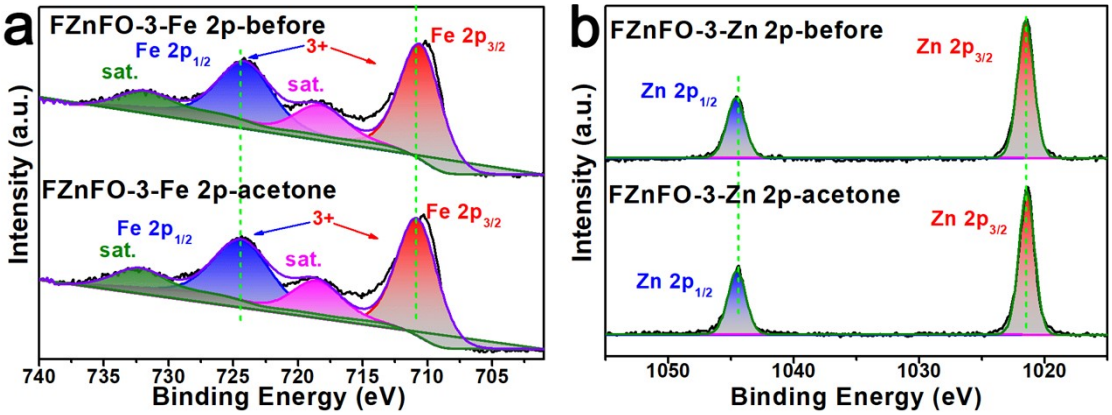

Fig. S8 The high-resolution XPS spectra before and after contact of FZnFO-3 samples with acetone at 170 ℃: Fe 2p (a), Zn 2p (b)

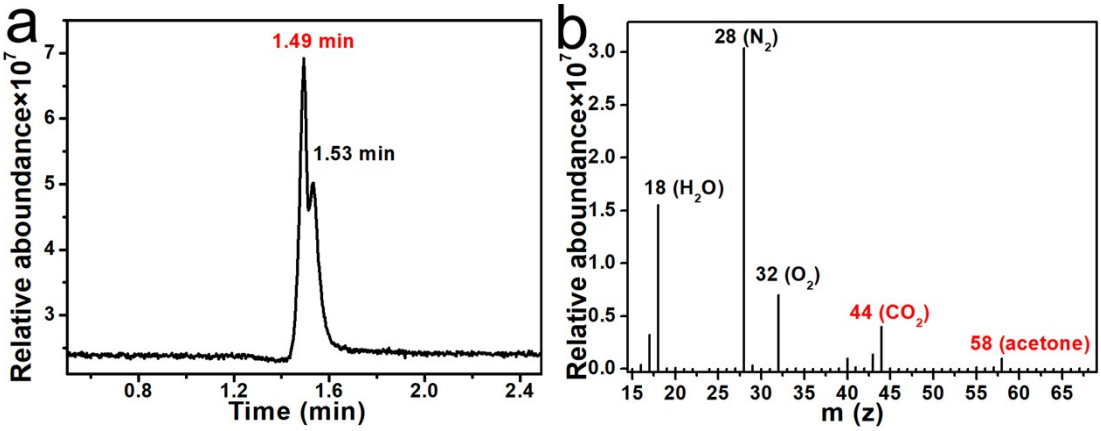

Fig. S9 Gas chromatogram (a) and mass spectra (b) of gaseous products of FZnFO-3 composite after contact with acetone gas

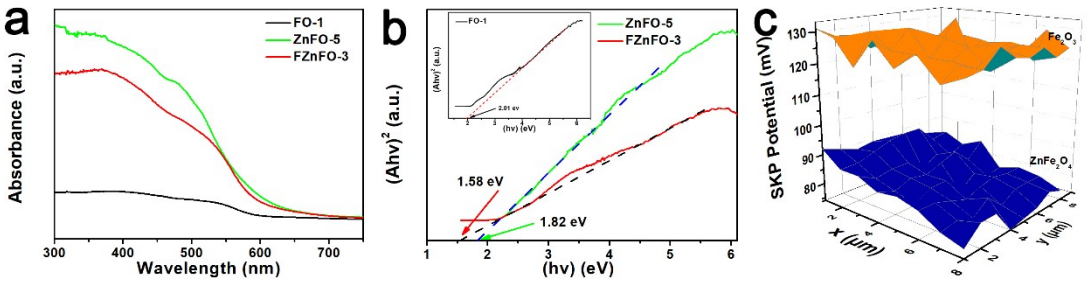

Fig. S10 UV absorption spectra (a-b) of $ZnFe_2O_4$, Fe_2O_3 and $ZnFe_2O_4/Fe_2O_3$. SKP potentials (c) of $ZnFe_2O_4$ and Fe_2O_3

The forbidden bandwidth (E_g) of $ZnFe_2O_4$, Fe_2O_3 and $ZnFe_2O_4/Fe_2O_3$ are calculated from the T_{auc} of the UV-Vis absorption spectrum (Fig. S10). Fig. S10b indicates that the E_g values of $ZnFe_2O_4$ and Fe_2O_3 are 1.82 eV and 2.01 eV, respectively. In addition, the forbidden bandwidth (1.58 eV) of the FZFO-3 composite can be seen to decrease, indicating that the chemical bonds between the different metal oxides are

interconnected and the material interfaces are in close contact, forming heterogeneous interfaces. According to the CPD data and calculations the work functions of $ZnFe_2O_4$ and Fe_2O_3 are 5.42 eV and 5.46 eV, respectively. (Fig. S10c).

Table S1 Recently reported sensors and their sensing performance for acetone gas

Sensing materials	Working temperature (°C)	Concentration (ppm)	response	Response/ recovery time (s)	Detection limit（ppm）	References
$Fe_2O_3/ZnFe_2O_4$	300	100 acetone	69.2	2/7	0.2	39
$ZnO/ZnFe_2O_4$	140	100 acetone	14.4	5.2/12.8	5	40
$ZnFe_2O_4/ZnO/Au$	225	100 acetone	30.8	1/58	0.3	41
$ZnFe_2O_4/ZnO$	290	100 acetone	25.8	8/32	1	42
$Fe_2O_3/ZnFe_2O_4$	170	100 acetone	62.8	6.8/146.2	0.02	This word

Table S2 Adsorption energy of acetone, TEA, and ethanol on $ZnFe_2O_4$ (400), $CaFe_2O_4$ (200), $CdFe_2O_4$ (220) surface

	The adsorption energy of acetone on the surface (eV)	The adsorption energy of TEA on the surface (eV)	The adsorption energy of ethanol on the surface (eV)
$ZnFe_2O_4$ (400)	-1.43	-0.92	-1.42
$CaFe_2O_4$ (200)	-1.07	-1.17	-0.98
$CdFe_2O_4$ (220)	-0.77	-0.86	-1.26